Fault Diagnosis for IGBTs Open-Circuit Faults in High-Speed Trains Based on Convolutional Neural Network

Huan Wang; Chun Zhang; Ning Zhang; Yiting Chen; Yaohua Chen
Engineering Research Center of Network Management Technology for High Speed Railway Ministry of Education
Beijing Jiaotong University
Beijing, China
17120416@bjtu.edu.cn

***Abstract*—Three-phase voltage source inverter is an important part of high-speed trains (HSTs) drive system. The stability of inverter directly affects the stability of motor speed control system and the safety of motor. IGBTs open-circuit faults are an important reason for the electrical faults of the inverters. Fault diagnosis is helpful to discover the cause of the fault in time and improve the safety and maintenance efficiency of HSTs. Most of the existing fault diagnosis methods need to build complex mathematical models or extract features from sensor signals manually. In order to solve these problems, the paper proposes a new method for IGBTs open-circuit fault diagnosis named Convolutional Neural Network for Extracting Comprehensive Information (CI-CNN) and a current signal to gray image conversion method named *k*-gray. In this paper, the three-phase current signals of traction motor stator are synchronously resampled by angle increment, and then the angle domain signals are transformed into gray image. CI-CNN extracts fault features from gray images to diagnose IGBTs open-circuit faults. The method does not need to extract fault features manually and achieves end-to-end fault diagnosis. Experiments show that the method has excellent adaptability in speed domains and load domains. At the same time, the combination of CI-CNN and *k*-gray has good diagnostic accuracy in noisy environment.**

Keywords-IGBTs Open-Circuit Faults; CI-CNN; k-gray; high-speed train; three-phase current;

I. INTRODUCTION

Inverter is responsible for converting direct current (DC) to alternating current (AC) and providing it to asynchronous motor. By controlling the switching frequency of IGBTs to output different voltage and torque, the AC speed regulation of motor can be realized. Space vector control can improve the control efficiency and is widely used in AC speed regulation system of high-speed trains (HSTs).

IGBT faults can be divided into open-circuit faults and short-circuit faults. Short circuit protection has become a standard of industrial drivers. When IGBTs open-circuit fault occurs, the inverter can still control the operation of traction motor, which is not easy to detect. According to the statistical results of HSTs faults, IGBTs open-circuit faults account for a large part of traction system faults. Online fault diagnosis of IGBTs can discover the faults in time, improve the driving safety of HSTs, prevent secondary injury, and the diagnosis results can guide the follow up maintenance and improve the maintenance efficiency of HSTs. Therefore, the research on IGBTs open-circuit fault diagnosis has attracted people's attention.

There are two main types of methods for IGBT open-circuit fault diagnosis, one is based on mathematical model, the other is based on feature extraction. Diagnostic methods based on mathematical models need to build complex mathematical models, and different circuit structures need to build different models. Reference [1] proposes a fault detection method based on state observer. The paper uses state observer to estimate the ideal circulating current and compares the ideal circulating current to the measured actual currents. If the difference between the ideal circulating current and the measured actual currents is lager than a proper threshold value I_{th} during the delay time ΔT_1, an open-circuit fault has occurred in the system. The method needs to design a good state observer, and select a proper I_{th} and ΔT_1. In [2], a mathematical model of current prediction is proposed, and fault diagnosis is carried out by comparing the processed current prediction value with a fault threshold value. In [3], a fault diagnosis algorithm based on the mathematical model is proposed. The algorithm detects open-circuit faults according to the different relationships between AC side output voltages and turn-on duty cycle of the corresponding IGBT under normal condition and fault condition. Reference [4] proposes an observer-based method for IGBTs fault diagnosis.

Fault diagnosis methods based on feature extraction mainly extract fault-related features from current or voltage. Generally, these methods need to extract features manually through Fourier transform or wavelet transform. In [5], The wavelet coefficients vector is extracted from stator current, then the wavelet coefficients are normalized and input into neural network for fault classification. Reference [6] uses wavelet transform to process time domain waveforms, and then obtains appropriate indexes to train an adaptive neuro-fuzzy inference system. Reference [7] uses wavelet transform to analyse stator current signals for IGBTs fault diagnosis. Reference [8] uses

This work was sponsored by the China Railway Corporation Program "Overall Technology Research of PHM for EMU"(No.K2018J018).

978-1-7281-0860-5/19/$31.00 ©2019 IEEE

fast Fourier transform to extract features from voltage signals, and uses principal component analysis to reduce the dimensions of samples. Finally, Reference [8] diagnoses the IGBTs open-circuit faults by Bayesian networks.

Besides, reference [9] uses the mean and entropy of three-phase current and three-phase voltage as features to train the neural network. Reference [10] diagnoses IGBTs faults based on the similarity of current. Reference [10] depends on the integrity of the waveform cycle, but in the stages of acceleration or deceleration of HSTs, the current signal is non-stationary, so it is difficult to obtain a complete cycle signal. Reference [11] designs a complex failure detection circuit to diagnose IGBTs open-circuit faults. The method introduces additional circuit to the system, increases the complexity of the system, and the fault diagnosis circuit also has the risk of failure.

According to the analysis above, in order to avoid building different mathematical models for different systems and extracting features manually, the main contributions of this paper are summarized as the following four points. Firstly, we propose a current signal to gray image conversion method named *k*-gray. Secondly, we construct a novel network framework named Convolutional Neural Network for Extracting Comprehensive Information (CI-CNN). The CI-CNN is an end-to-end IGBTs open-circuit fault diagnosis method. The method does not need additional sensors, feature extraction methods and setting fault thresholds which need a lot of expert knowledge to determine, nor does it depends on the integrity of current cycle. Thirdly, according to the experimental results, compared with other diagnostic systems, this method has good adaption ability of speed domains and load domains. Fourthly, experiments show that *k*-gray can effectively improve the anti-noise ability of CI-CNN.

The rest of this paper is organized as follows. Section II discusses the related works of fault diagnosis based on convolutional neural network (CNN). Section III presents the fault diagnosis system based on CI-CNN, including how to improve signal-to-image conversion method and the architecture of CI-CNN. In Section IV, experiments show the performance of the proposed diagnostic system and compare it with other diagnostic systems. The conclusion and future research works are presented in the Section V.

II. Related Works

This section discusses the related works of fault diagnosis based on CNN.

CNN has the functions of feature extraction and classification, and can realize end-to-end diagnosis. Therefore, intelligent diagnosis algorithms based on CNN have been paid more and more attention.

Reference [12] proposes a fault diagnosis system based on LeNet-5. Firstly, reference [12] converts the time domain raw signals into images which are set as 64-by-64, then these images feed into CNN. According to [12], the method outperforms traditional methods. Reference [13] proposes a novel method named Deep Convolutional Neural Networks with Wide First-layer Kernels (WDCNN) for fault diagnosis on raw vibration signals. WDCNN has better performance under different working load and noisy environment conditions. Reference [14] proposes deeper 1D convolutional neural network (Der-1DCNN) which combines CNN with residual learning for fault diagnosis of high-speed gear box. Experiments show that the method is quite superior under the condition of strong noise and varying working loads. Reference [15] incorporates data from multiple sensors, and feeds the data into CNN to achieve higher and more robust diagnosis accuracy. Reference [16] proposes a new multiscale convolutional neural network architecture which performs multiscale feature extraction to automatically identify different health conditions of wind turbine gearbox.

Some researchers use transfer learning to diagnose faults. Reference [17] trains the neural networks by working condition 1 which has enough data, then retrains the networks by a small amount of data in working condition 2. The result shows that the neural network has a good classification accuracy for working condition 2. Reference [18] uses transfer learning to realize preprocessing-free gear fault diagnosis. Reference [19] uses ResNet-50 trained on ImageNet as feature extractor, then converts time-domain fault signals to RGB images as the input data of ResNet-50 for fault diagnosis.

III. Proposed Fault Diagnosis System Based on CI-CNN

This section introduces IGBTs open-circuit fault diagnosis system based on CI-CNN. Firstly, the method of three-phase current signals resampled synchronously is detailed. Secondly, the method of conversing three-phase current signals to gray images is presented. Finally, the architecture of CI-CNN is detailed.

A. Three-phase current signals resampled synchronously

During the acceleration and deceleration stages of HSTs, the three-phase current of traction motor stator is non-stationary. In addition, three-phase current has different frequencies under different speed of traction motor. In order to reduce the influence of different rotational speed of traction motor on the diagnosis results, three-phase current signals are sampled synchronously in angle domain. In this paper, 1000 points are collected for each rotation of traction motor. If the speed of motor is n rpm, and the time interval between adjacent sampling points is t_{in} seconds, then t_{in} is calculated as

$$t_{in} = \frac{60}{n \times 1000} \, seconds. \tag{1}$$

In order to reduce the computational load, this paper assumes that HSTs run at a uniform speed in t_{in} seconds. The rated speed of traction motor of CRH1, CRH2, CRH3 are 2725 rpm, 4140 rpm, 4100 rpm respectively [20]. When n is small, the change of speed in t_{in} seconds is relatively small. When n is large, for example, if n=2000 rpm, then t_{in} = 0.00003 seconds, so this assumption is acceptable. At the same time, the raw three-phase current signals can be very long, in order to make full use of the information of the raw signal, we use a sample window to collect sample points. The length of sample window is smaller than the length of raw current signal.

Through sliding the sample window, we can obtain more images. The step size t_{sli} is little, in this paper, t_{sli} is 0.002 seconds. For the raw three-phase current signals and velocity signals, the whole synchronous resampling algorithm is:

1) The time of the first sampling point t_{init} is the time of the first point of the raw current signal.

2) If the current sampling time is t_{sli}, the current speed is s_{cur} rpm, then the next sampling time t_{next} can be calculate as

$$t_{next} = t_{cur} + \frac{s_{cur}}{60 \times 1000} \ seconds. \tag{2}$$

3) $t_{cur}=t_{next}$, Repeat step 2) until the sample points meet the requirement of converting to gray image. In this paper, the requirement is 500.

4) $t_{init}=t_{init}+t_{sli}$, Repeat step 2), 3) and collect the sample points of the next image.

In Fig. 1, a) and c) are equal in time. a) shows the raw current signal when the rotation rate of traction motor slows down from 1000 rpm to 400 rpm under health condition, c) shows the raw current signal when the rotation rate of traction motor is constant at 400 rpm under health condition, b) and d) are the results of a) and c) resampling respectively. From Fig. 1, we can see that there are great differences between a) and c) while b) and d) are very similar in shape. Therefor the resampling method is helpful for the subsequent fault diagnosis.

B. *Three-phase current signal to gray images conversion method*

Reference [12] converts 1D vibration signals into 2D gray images. Experiments show that this method can extract fault features effectively. Reference [19] converts time-domain fault signals to the RGB format images. In these two papers, a segment signal with the length M^2 which is randomly obtained from the raw signal is evenly divided into M parts. Each part is used to generate a row of pixels of an image. In the two papers, both the raw signals are 1D, therefore, this method does not lose the structure information of the raw vibration signals. However, the three-phase current signals are 3D, and the time of 500 sample points is approximately equal to the time of one cycle of the raw current signals. If this method is used to convert current signals, the periodic information of the signal itself and the information of the interaction between three-phase currents will be lost. To solve this problem, we use 500 sample points to generate a gray image, the size of the image is 500-by-3. S_{ik}, i=1,2,...,500, k=1,2,3 denotes the 500 sample points, S_{i1}, S_{i2} and S_{i3} separately denote A phase current, B phase current, C phase current. P_{ik}, i=1,2,...,500, k=1,2,3 denotes the pixel strength of the image. *Min* and *Max* denote the maximum value and minimum value of S_{ik}, respectively. The function round(.) is the rounding function and the whole pixel value has been normalized from 0 to 255. This method is named *d*-gray because each sample point is directly converted into gray value.

$$P_{ik} = round\left(\frac{S_{ik} - Min}{Max - Min} \times 255\right) \tag{3}$$

For the test dataset, considering that the three-phase current may be disturbed by noise, the raw current signal is processed according to (4), and then convert it to gray images according to (3).

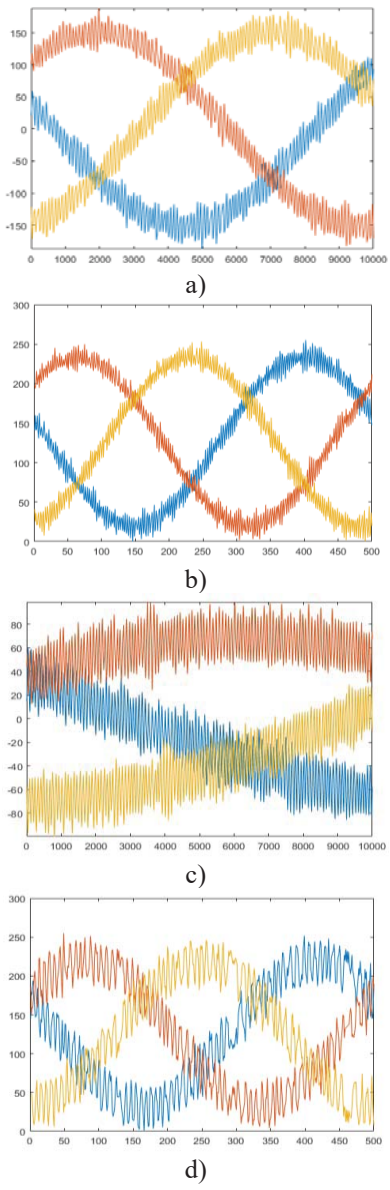

Figure 1. Three-phase current signals a) The rotation rate of traction motor slows down from 1000rpm to 400 rpm under health condition b) The results of a) synchronous resampling c) The rotation rate of traction motor is constant at 400 rpm under health condition d) The results of c) synchronous resampling

$$S_{ik} = \frac{1}{s_1 + s_2 + 1} \sum_{j=i-s_2}^{j=i+s_1} S_{jk} \tag{4}$$

i=s_2+1, s_2+2,…,500-s_1. In the paper, s_1=s_2=7. Through (4), the interference of noise in raw current signal to fault diagnosis can be reduced. This method is named *k*-gray because each sample point is equal to the average value of its k adjacent sample points.

C. *The architecture of CI-CNN*

The operating conditions of HSTs are complex. This

requires that the fault diagnosis method can adapt to the speed and load changes of HSTs. CNN has a strong abstraction ability. However, if the CNN is too deep, it is easy to fall into over-fitting and does not adapt to the changing working conditions while the shallow CNN is easy to fall into under-fitting, and dose not effectively extract fault-related features. To solve these problems, the architecture of CI-CNN is shown in Fig. 2.

1) Input: The input of CI-CNN is the gray images generated by the raw current signals. Before feature learning, each batch of images is processed by batch normalization (BN). BN normalizes its inputs x_i by first calculating the mean μ_B and variance σ_B^2 over a mini-batch. It calculates the normalized activations as

$$\hat{x}_i = \frac{x_i - \mu_B}{\sqrt{\sigma_B^2}} \tag{5}$$

$$y_i = \gamma \cdot \hat{x}_i + \beta \tag{6}$$

β and γ are offset and scale properties respectively. y_i is the output of x_i.

2) Feature learning: The convolutional layer is composed of a number of filters. Each filter moves along the input image vertically and horizontally, repeating the same computation for each region. W_i^l and b_i^l denote the weights and bias of the i-th filter in layer l, respectively, $x^{l-1}(j)$ denotes the j-th region in layer l-1.

$$y_i^l(j) = W_i^l * x^{l-1}(j) + b_i^l \tag{7}$$

$y_i^l(j)$ denotes the output of $x^{l-1}(j)$ calculated by i-th filter. * is an operator of convolution.

In order to extract the comprehensive information of three-phase current, ConvolutionLayer1 and ConvolutionLayer2 adopt convolution filters whose width equals to the width of gray images. Because the gray images contain noise and useless information, the filters of ConvolutionLayer1 have a larger stride (4-by-1) in the angle direction. With the deepening of the network, the correlation between the information extracted by CI-CNN and the fault gradually increases. In order not to lose useful information, the filters of ConvolutionLayer2, ConvolutionLayer3 have a stride of 1-by-1.

Output of convolution layers are also processed by BN layer. The results of BN layer are input into rectified linear unit (ReLU) layer. A ReLU layer performs a threshold operation to each element of the input, where any value less than zero is set to zero.

Average pooling layers perform down-sampling by dividing the input into rectangular pooling regions and computing the average values of each region. In order to reduce noise interference and avoid over-fitting, the size and stride of the filters in AveragePoolingLayer1, AveragePoolingLayer2 separately are 2-by-1 and 1-by-1. The size and stride of the filters in AveragePoolingLayer3 are 2-by-1.

3) Classification: Output of AveragePoolingLayer3 is reshaped as 1D and fed into fully-connected layer. The fully-connected layer uses sofmax function to classify. The loss function of CI-CNN is the cross entropy, which is calculates as

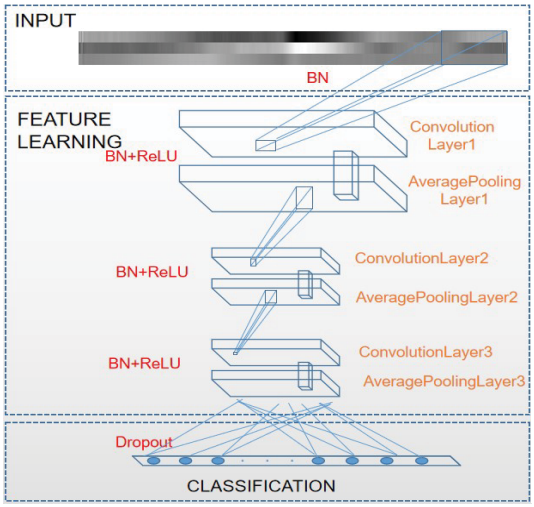

Figure 2. The architecture of CI-CNN

$$loss = -\sum_{i=1}^{N}\sum_{j=1}^{K} t_{ij} \ln y_{ij}. \tag{8}$$

where N is the number of samples, K is the number of classes, t_{ij} is the indicator that i-th sample belongs to the j-th class, y_{ij} is the output for sample i for class j.

4) Parameters: The parameters of the CI-CNN are detailed in Table I.

D. CI-CNN based fault diagnosis

As shown in Fig. 3, the overall procedure is summarized as follows.

1) The three-phase current signals of traction motor stator are collected by current sensors.

2) The three-phase current signals collected are resampled from time increments to angle increments.

3) The training dataset is transformed into gray images by d-gray, and the test dataset is transformed into gray images by

TABLE I. PARAMETERS OF CI-CNN

Name	The Size of Filters	The Stride of Filters	The Number of Filters	Padding
Convolution Layer1	3×3	4×1	64	same
AveragePooling Layer1	2×1	1×1	64	same
Convolution Layer2	2×3	1×1	64	no
AveragePooling Layer2	2×1	1×1	64	same
Convolution Layer3	2×1	1×1	64	no
AveragePooling Layer3	2×1	2×1	64	no

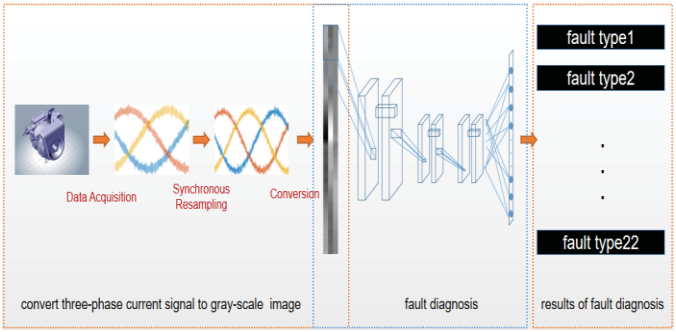

Figure 3. The overall procedure of IGBTs open-circuit fault diagnosis

k-gray. The test dataset and training dataset contain different working conditions respectively, and the two data datasets have no intersection.

4) The training dataset is used to train CI-CNN, and the test dataset is used to evaluate the classification accuracy and domain adaptability of the network.

IV. Experimental Evaluation

In this section, the vector control system of traction motor is simulated with MATLAB/Simulink to obtain fault data. The proposed fault diagnosis method is validated by the obtained fault data.

A. Experimental Setups

1) Simulation: In order to ensure the objectivity of the experimental results, this paper uses the model named Field-Oriented Control Induction 200 HP Motor Drive provided by MATLAB. The simulation model is shown in Fig. 4. The main circuit of the model is "AC-DC-AC" structure. The three-phase voltage source inverter is connected with the traction motor. The speed controller is based on a PI regulator. The outputs of this regulator are set points for the torque and the flux applied to the Field Oriented Controller (FOC) block. When the speed of motor is lower than the rated value, the flux instruction is the rated value. When the speed of motor is higher than the rated value, the flux instruction is inversely proportional to the speed of motor.

2) Data acquisition: The main circuit of the inverter is shown in Fig. 5. The inverter has six IGBTs. This paper assumes that at most two IGBTs fail simultaneously, then all types of open-circuit faults are shown in Table II. We use the simulation model to obtain the fault data under different working conditions. All working conditions are shown in Table III. 22 kinds of IGBTs open-circuit faults are simulated under each working condition. There are 50 gray images for each IGBTs open-circuit fault in each working condition. The training dataset includes Con 1, Con 3, Con 11, Con 13, Con 14, others are test dataset.

3) Baseline system:

a) CS: The method is proposed in [10] which uses discrete wavelet transform to obtain fault features from three-phase current, then Euclidean distance between every two of the fault features are calculated for measuring the current similarity to diagnose fault [10]. According to [10], the

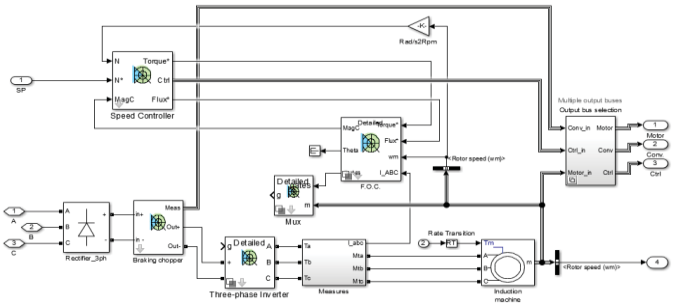

Figure 4. Internal structure of vector control asynchronous motor drive system module

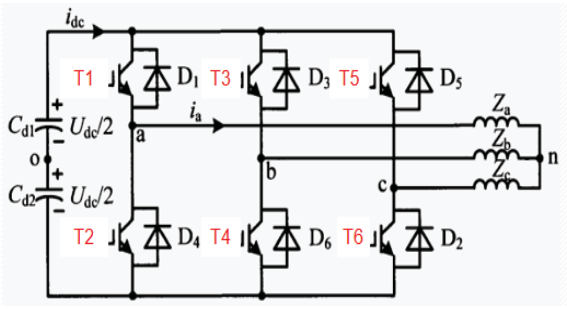

Figure 5. The main circuit of three-phase voltage source inverter

TABLE II. IGBT Open-circuit Fault Types

Health Conditions	Fault Location
Health	None
Single IGBT Fail	T1,T2,T3,T4,T5,T6
Double IGBT Fail	T1T2,T1T3,T1T4,T1T5,T1T6,T2T3, T2T4,T2T5,T2T6,T3T4,T3T5,T3T6, T4T5,T4T6,T5T6

TABLE III. WORKING CONDITIONS

Working Conditions	Speed (rpm)	Load (Nm)	Name
Uniform Speed	200	0	Con 1
	200	200	Con 2
	200	300	Con 3
	300	0	Con 4
	300	100	Con 5
	300	200	Con 6
	400	0	Con 7
	400	200	Con 8
	400	400	Con 9
	600	0	Con 10
	1000	0	Con 11
Acceleration (Initial speed/Final speed)	50/500	0	Con 12
	100/1000	0	Con 13
Deceleration (Initial speed/Final speed)	800/300	0	Con 14
	1000/400	0	Con 15

method needs to compare the fault index with the threshold value that is determined by experience. Different traction motors need to determine different thresholds, which makes the method difficult to apply. Therefore, we improve fault diagnosis conditions of the method. The improved fault diagnosis conditions are shown in Table IV. r_{ij} is the similarity between the i phase current and the j phase current, Sum_i is the mean of the wavelet coefficients of the i phase current. The original method and the improved method are called CS1 and CS2 respectively. It is worth noting that CS1 and CS2 only diagnose faults proposed by [10], because the number of fault types proposed by [10] is less than that in this paper.

b) WDCNN: WDCNN is proposed by [13]. Because WDCNN is used to process 1D vibration signals, in order to process three-phase current signals, the size of the first layer convolution filters of WDCNN is set as 16-by-3, and the other layers remain unchanged.

c) CNN1: All convolution filters of CNN1 have a length of 1 in the direction of phase current. CNN1 can be used to compare the performance differences of extracting comprehensive information of three-phase current and extracting each phase current information separately.

d) AlexNet: AlexNet is a convolutional neural network that is trained on more than a million images from the ImageNet database. We use AlexNet to discuss the effect of transfer learning in IGBTs open-circuit fault diagnosis. IGBTs open-circuit faults data is used to fine-tune it. Because the network has an image input size of 227-by-227, we use (9) to process resampled signals, and save the result as 227-by-227 images. Some of the images are shown in Fig. 6.

$$S_{ik}=\begin{cases}\dfrac{S_{ik}-Min_k}{Max_k-Min_k}+1 & if\ k=1\\ \dfrac{S_{ik}-Min_k}{Max_k-Min_k} & if\ k=2\\ \dfrac{S_{ik}-Min_k}{Max_k-Min_k}-1 & if\ k=3\end{cases} \tag{9}$$

S_{ik} is denotes resampled signal. k=1,2,3 denotes A phase current, B phase current and C phase current, respectively. Min_k is denotes the minimum value of k phase current. Max_k is denotes the maximum value of k phase current.

TABLE IV. FAULT DIAGNOSIS CONDITIONS

Current similarity	Accumulated coefficient	Faulty IGBT
$r_{ab}=r_{bc}=r_{ac}$	X	No
$r_{bc}<r_{ab}, r_{bc}<r_{ac},$	Sum_a<-50	T1
$r_{bc}<r_{ab}, r_{bc}<r_{ac}$	Sum_a>50	T2
$r_{bc}<r_{ab}, r_{bc}<r_{ac}$	-50<Sum_a<50	T1T2
$r_{ac}<r_{bc}, r_{ac}<r_{ab}$	Sum_b<-50	T3
$r_{ac}<r_{bc}, r_{ac}<r_{ab}$	Sum_b>50	T4
$r_{ac}<r_{bc}, r_{ac}<r_{ab}$	-50<Sum_b<50	T3T4
$r_{ab}<r_{ac}, r_{ab}<r_{bc}$	Sum_c<-50	T5
$r_{ab}<r_{ac}, r_{ab}<r_{bc}$	Sum_c>50	T6
$r_{ab}<r_{ac}, r_{ab}<r_{bc}$	-50<Sum_c<50	T5T6

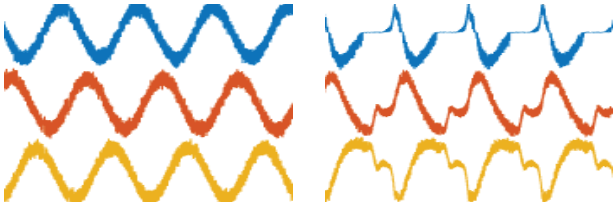

a) b)

Figure 6. a) No fault under Con 6. b) T1 fails under Con 6

B. *Case Study1:Speed Domains Adaption*

Because the speed conditions of HSTs are various, the diagnosis algorithm must have good speed domains adaptability. The fault diagnosis results are shown in Table V.

From the diagnosis results, we can see that the lowest accuracy of CI-CNN is 99.91%, and AlexNet is 100%, so CI-CNN and AlexNet have excellent speed domains adaptability. Compared with AlexNet, CI-CNN has faster diagnostic speed and less computational load. The accuracy of CS1 is very low. The main reason is that the threshold given by [10] depends heavily on the working conditions. The lowest accuracy of CS2 is 24.44% and the highest is 80.60%, which is better than CS1. This proves that the improvement of CS1 is effective. WDCNN has poor diagnostic effect, which indicates that wide convolution filters are not suitable for IGBTs open-circuit fault diagnosis. The diagnostic effect of CNN1 is worse than that of CI-CNN, which proves that extracting comprehensive information of three-phase current is better than extracting information of each phase current separately.

C. *Case Study2:Load Domains Adaption*

The load of HSTs is also various, so the fault diagnosis system must have good load domains adaptability. According to the above analysis, WDCNN and CS1 are not suitable for IGBTs open-circuit fault diagnosis, in the remaining cases, only the other methods are compared. The fault diagnosis results are shown in Table VI.

The result shows that the accuracy of CI-CNN is close to 100% under all working conditions. The accuracy of AlexNet and CNN1 is similar, and both have poor diagnostic effect on Con 9. Moreover, the accuracy of AlexNet and CNN1 decreases with the increase load. The main reason is that the amplitude of the current waveform varies with the load. Moreover, when open-circuit fault occurs, the current waveform will be distorted, and the amplitude and position of the waveform distortion will be different under different loads. Therefore, when the same fault occurs, the waveforms are

different under different loads, which makes the accuracy of fault diagnosis decrease. Besides, in terms of accuracy, there is a significant gap between CS2 and other fault diagnostic systems.

D. Case Study3:Anti-Noise Ability

The running environment of HSTs is complex, and the three-phase current may be disturbed by noise. Therefore, the anti-noise ability of fault diagnosis system must be paid attention to. We add white Gaussian noise with signal-to-noise ratio (SNR) of 2, 4, 6, 8 and 10 to the resampled current signals. The anti-noise ability of the fault diagnosis systems is shown in Table VII.

As the results show, the anti-noise ability of CI-CNN is superior to other fault diagnosis systems. When SNR = 2 db, CI-CNN can achieve more than 96% accuracy in most cases. AlexNet has the worst anti-noise ability. This indicates that AlexNet's generalization ability is poor. The reason may be that AlexNet has too high feature extraction ability, which leads to a certain degree of over-fitting. We also compare *k*-gray and *d*-gray methods. As shown in Table VIII, under Con 4, the lowest accuracy of *k*-gray+CI-CNN and *d*-gray+CI-CNN is 96.36% and 88.64%, respectively. *k*-gray significantly improves the anti-noise ability of CI-CNN. The main reason is that noise causes various distortion of current waveform, and *k*-gray makes the value of each sample point equal to the average value of its *k* neighbor sample points, which weakens the influence of noise on diagnosis results.

TABLE V. THE FAULT DIAGNOSIS RESULTS OF CASE STUDY1

Fault Diagnosis Systems	Con 4	Con 7	Con 10	Con 12	Con 15
CI-CNN	100%	100%	100%	100%	99.91%
CS1	9.4%	7.4%	9.8%	9.4%	7.6%
CS2	68%	80.4%	80.8%	65.8%	27.2%
WDCNN	4.55%	4.55%	4.55%	4.55%	4.55%
AlexNet	100%	100%	100%	100%	100%
CNN1	79.64%	92.82%	96.64%	99.18%	80.09%

TABLE VI. THE FAULT DIAGNOSIS RESULTS OF CASE STUDY2

Fault Diagnosis Systems	Con 2	Con 5	Con 6	Con 8	Con 9
CI-CNN	100%	100%	99.91%	99.91%	100%
CS2	59.2%	79.8%	78.4%	77.2%	87.2%
AlexNet	100%	97.18%	100%	99.64%	95.18%
CNN1	99.09%	99.18%	99.09%	98.91%	97.64%

TABLE VII. THE FAULT DIAGNOSIS RESULTS OF CASE STUDY3

Conditions	SNR(db)	CI-CNN	CS2	AlexNet	CNN1
Con 4	2	96.36%	62.6%	9.55%	69.73%
	4	99.09%	64%	19.55%	73.27%
	6	99.09%	63.2%	30.73%	76.18%
	8	99.91%	64.2%	45.45%	75.27%
	10	100%	63%	63.27%	76.27%
Con 6	2	96.45%	69.2%	10.45%	73.73%
	4	98.55%	71.8%	12.27%	83.64%
	6	99.36%	71.2%	19%	88.91%
	8	99.55%	73.2%	33.82%	92.36%
	10	99.73%	75%	43.18%	93.82%
Con 12	2	97.18%	66%	10.82%	75.18%
	4	98%	66%	15.82%	80.09%
	6	99.09%	67%	24.36%	83.82%
	8	99.36%	68.8%	35.82%	87.55%
	10	99.64%	68%	41.73%	90.82%
Con 15	2	90.73%	29.6%	8.73%	55.36%
	4	96.27%	28%	8.27%	69.36%
	6	99.09%	26.8%	11.45%	78.18%
	8	99.55%	25.2%	18.27%	84.55%
	10	100%	26.6%	23.82%	86.91%

TABLE VIII. THE FAULT DIAGNOSIS RESULTS OF K-GRAY+CI-CNN AND D-GRAY+CI-CNN UNDER CON 4

SNR(db)	*k*-gray+CI-CNN	*d*-gray+CI-CNN
2	96.36%	88.64%
4	99.09%	95.55%
6	99.09%	95.91%
8	99.91%	99.73%
10	100%	100%

V. CONCLUSION

This paper proposes a new IGBTs open-circuit fault diagnosis system based on CI-CNN. CI-CNN extracts comprehensive information of three-phase current for fault diagnosis. Compared with the existing methods, CI-CNN achieves end-to-end fault diagnosis without using traditional feature extraction methods, and it doesn't need to set fault thresholds and depend on the integrity of current cycle.

Through the experiment, we use the data of some working conditions to train network, and use the data of other working conditions to test. The results show that CI-CNN has strong robustness. It has excellent speed domains and load domains adaptability without adjusting network structure and parameters. At the same time, the performance of CI-CNN in noisy environment is also discussed. The results show that the combination of *k*-gray and CI-CNN has good anti-noise ability.

We also discuss the effect of transfer learning in IGBTs open-circuit fault diagnosis through AlexNet. The results show that AlexNet has good diagnostic accuracy in noiseless

environment, but it has poor diagnostic accuracy in noisy environment. This shows AlexNet has strong feature extraction capabilities, which results in poor domain adaptation ability and anti-noise ability.

This paper only focuses on the open-circuit faults of IGBTs in other parts of traction converter under normal conditions. Future research will focus on how to accurately diagnose the open-circuit faults of IGBTs when other parts of traction converter fail.

REFERENCES

[1] B. Li, S. Shi, B. Wang, G. Wang, W. Wang and D. Xu, "Fault Diagnosis and Tolerant Control of Single IGBT Open-Circuit Failure in Modular Multilevel Converters," in IEEE Transactions on Power Electronics, vol. 31, no. 4, pp. 3165-3176, April 2016.

[2] P. Sobanski and T. Orlowska-Kowalska, "IGBT open-circuit fault diagnosis based on the current prediction in the line-side AC/DC converter," 2017 IEEE International Conference on Industrial Technology (ICIT), Toronto, ON, 2017, pp. 113-118.

[3] H. Zhang, C. da Sun, Z. Li, J. Liu, H. Cao and X. Zhang, "Voltage Vector Error Fault Diagnosis for Open-Circuit Faults of Three-Phase Four-Wire Active Power Filters," in IEEE Transactions on Power Electronics, vol. 32, no. 3, pp. 2215-2226, March 2017.

[4] I. Jlassi, J. O. Estima, S. K. El Khil, N. M. Bellaaj and A. J. M. Cardoso, "A Robust Observer-Based Method for IGBTs and Current Sensors Fault Diagnosis in Voltage-Source Inverters of PMSM Drives," IEEE Transactions on Industry Applications, vol. 53, no. 3, pp. 2894-2905, May-June 2017.

[5] F. Charfi, F. Sellami and K. Al-Haddad, "Fault Diagnostic in Power System Using Wavelet Transforms and Neural Networks," 2006 IEEE International Symposium on Industrial Electronics, Montreal, Que., 2006, pp. 1143-1148.

[6] M. A. Awadallah and M. M. Morcos, "Diagnosis of switch open-circuit fault in PM brushless DC motor drives," Large Engineering Systems Conference on Power Engineering, 2003, Montreal, Quebec, Canada, 2003, pp. 69-73.

[7] M. Aktas and V. Turkmenoglu, "Wavelet-based switching faults detection in direct torque control induction motor drives," in IET Science, Measurement & Technology, vol. 4, no. 6, pp. 303-310, November 2010.

[8] B. Cai, Y. Zhao, H. Liu and M. Xie, "A Data-Driven Fault Diagnosis Methodology in Three-Phase Inverters for PMSM Drive Systems," in IEEE Transactions on Power Electronics, vol. 32, no. 7, pp. 5590-5600, July 2017.

[9] M. Alavi, M. Luo, D. Wang and H. Bai, "IGBT fault detection for three phase motor drives using neural networks," Proceedings of 2012 IEEE 17th International Conference on Emerging Technologies & Factory Automation (ETFA 2012), Krakow, 2012, pp. 1-8.

[10] H. Yang, J. Zhao and F. Wu, "Current similarity based fault diagnosis for induction motor drives with discrete wavelet transform," 2016 Prognostics and System Health Management Conference (PHM-Chengdu), Chengdu, 2016, pp. 1-6.

[11] M. A. Rodríguez-Blanco, A. Vázquez-Pérez, L. Hernández-González, V. Golikov, J. Aguayo-Alquicira and M. May-Alarcón, "Fault Detection for IGBT Using Adaptive Thresholds During the Turn-on Transient," in IEEE Transactions on Industrial Electronics, vol. 62, no. 3, pp. 1975-1983, March 2015.

[12] L. Wen, X. Li, L. Gao and Y. Zhang, "A New Convolutional Neural Network-Based Data-Driven Fault Diagnosis Method," IEEE Transactions on Industrial Electronics, vol. 65, no. 7, pp. 5990-5998, July 2018.

[13] Zhang W, Peng G, Li C, Chen Y, Zhang Z, "A New Deep Learning Model for Fault Diagnosis with Good Anti-Noise and Domain Adaptation Ability on Raw Vibration Signals," Sensors, vol. 17, pp. 425-446, Feb 2017.

[14] D. Peng, Z. Liu, H. Wang, Y. Qin and L. Jia, "A Novel Deeper One-Dimensional CNN With Residual Learning for Fault Diagnosis of Wheelset Bearings in High-Speed Trains," IEEE Access, vol. 7, pp. 10278-10293, 2019.

[15] M. Xia, T. Li, L. Xu, L. Liu and C. W. de Silva, "Fault Diagnosis for Rotating Machinery Using Multiple Sensors and Convolutional Neural Networks," IEEE/ASME Transactions on Mechatronics, vol. 23, no. 1, pp. 101-110, Feb. 2018.

[16] G. Jiang, H. He, J. Yan and P. Xie, "Multiscale Convolutional Neural Networks for Fault Diagnosis of Wind Turbine Gearbox," IEEE Transactions on Industrial Electronics, vol. 66, no. 4, pp. 3196-3207, April 2019.

[17] R. Zhang, H. Tao, L. Wu and Y. Guan, "Transfer Learning With Neural Networks for Bearing Fault Diagnosis in Changing Working Conditions," IEEE Access, vol. 5, pp. 14347-14357, 2017.

[18] Cao P , Zhang S , Tang J, "Pre-Processing-Free Gear Fault Diagnosis Using Small Datasets with Deep Convolutional Neural Network-Based Transfer Learning," IEEE Access, pp. 26241-26253, 2017.

[19] Wen L , Li X , Gao L, "A transfer convolutional neural network for fault diagnosis based on ResNet-50," Neural Computing and Applications, pp. 1-14, 2019.

[20] Xiquan Z. Train Electric Drive and Control. China: Southwest Jiaotong University Press, 2010, pp. 251-252.